LA-UR-04-4327

Title: An Overview of Relativistic Distorted-Wave Cross Sections

Author(s): Christopher J. Fontes, Hong Lin Zhang and Joseph Abdallah, Jr.

Submitted to: Conference Proceedings for the 14th APS Topical Conference on Atomic Processes in Plasmas

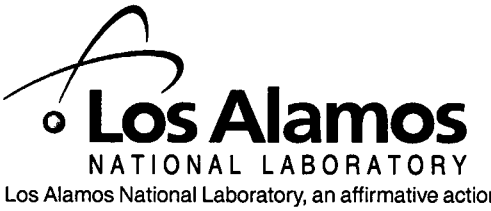

An Overview of Relativistic Distorted-Wave Cross Sections

Christopher J. Fontes, Hong Lin Zhang and Joseph Abdallah, Jr.

Los Alamos National Laboratory, P.O. Box 1663, Los Alamos, NM 87545

Abstract. Over the past twenty years significant progress has been made in calculating the vast amounts of relativistic atomic data that are required to model heavy element, non-LTE plasmas. A number of the relevant processes, including electron-impact excitation, photoionization, autoionization and electron-impact ionization, involve the computation of continuum electron wavefunctions. If the plasma consists of ions with sufficiently high charge, then the distorted-wave approximation is valid and can be used to compute these continuum orbitals and the corresponding cross sections. An overview of the relativistic distorted-wave approach is provided with an aim toward underscoring the similarities and differences with the longer established, nonrelativistic and semi-relativistic approaches. An example for extending the distorted-wave approach to less highly charged systems via the inclusion of resonance contributions to the cross sections is provided. Related topics, such as the top-up contribution, the high energy (Bethe) cross section limit, the Breit and Møller interactions, and transitions among magnetic sublevels are also discussed.

INTRODUCTION

The use of fully relativistic atomic data in plasma modeling becomes increasingly important with increasing atomic number Z. Some examples of applications that benefit from a fully relativistic treatment include the spectroscopic analysis of stars (iron, Z=26), fluorescent lighting technology (xenon, Z=54), inertial confinement fusion (gold, Z=79) and nuclear stockpile stewardship (uranium, Z=92). The Los Alamos National Laboratory (LANL) relativistic distorted-wave (RDW) effort was developed to provide data for modeling plasmas of this nature and is strongly based on the research program developed by Douglas Sampson and coworkers at Penn State University [e.g. 1–3]. A review article of this research is currently being written [4] in order to capture the breadth of this work in one convenient publication. The two guiding precepts of this program are to develop

computer codes that are (1) fast, and yet (2) provide accurate data within the RDW paradigm. As is true of all DW formalisms, the resulting RDW data are expected to be most accurate for highly charged ions, for which the electron-electron interaction is considered to be a perturbation relative to the nuclear Coulomb interaction.

BASIC THEORY AND COMPUTATIONAL FRAMEWORK

The theory of the RDW approach can be found in [1–3] and the references provided therein. The fundamental difference between this fully relativistic approach and other non- or semi-relativistic approaches is that all (i.e. both bound and free) electron wavefunctions are solutions of some form of the many-electron Dirac equation rather than the Schrödinger equation. For example, each bound electron wavefunction can be written in the form of a Dirac spinor

$$u_{n\kappa m}(x) = \frac{1}{r}\begin{bmatrix} P_{n\kappa}(r) & \chi_{\kappa m}(\theta,\phi,\sigma) \\ iQ_{n\kappa}(r) & \chi_{-\kappa m}(\theta,\phi,\sigma) \end{bmatrix}, \tag{1}$$

with large and small components (P and Q, respectively) that are solutions of the coupled differential equations

$$\left[\frac{\mathrm{d}}{\mathrm{d}r} + \frac{\kappa}{r}\right] P_{n\kappa}(r) = \frac{\alpha}{2}\left[\epsilon_{n\kappa} - V(r) + \frac{4}{\alpha^2}\right] Q_{n\kappa}(r) \tag{2}$$

and

$$\left[\frac{\mathrm{d}}{\mathrm{d}r} - \frac{\kappa}{r}\right] Q_{n\kappa}(r) = \frac{\alpha}{2}(V(r) - \epsilon_{n\kappa}) P_{n\kappa}(r)\,. \tag{3}$$

In the above equations the $\chi_{\kappa m}$ functions are the usual spin-angular-momentum functions, κ is the relativistic quantum number that takes on the values

$$\kappa = \ell, \quad j = \ell - \tfrac{1}{2}; \quad \kappa = -(\ell+1), \quad j = \ell + \tfrac{1}{2}\,, \tag{4}$$

$\epsilon_{n\kappa}$ is the energy eigenvalue, $V(r)$ represents the nuclear and electron-electron potentials and α is the fine structure constant. A similar set of expressions applies to the continuum electron wavefunctions except that the principal quantum number n is replaced with a continuous variable to represent the free-electron energy.

The capability to solve such systems of equations and provide fully relativistic data is contained within the LANL suite of atomic data codes [5–7]. Vast amounts of data are required to carry out plasma kinetics modeling and these codes provide the cross sections associated with a variety of atomic processes (and their inverses), which include photoexcitation (radiative decay), photoionization (radiative recombination), collisional excitation (collisional de-excitation), collisional

ionization (three-body recombination) and autoionization (di-electronic capture). For the purpose of this work numerical results for only collisional excitation and collisional ionization will be discussed in some detail, with autoionization being mentioned in connection with the resonance contribution to collisional excitation. The emphasis of the following discussion concerns extensions and improvements to the basic types of RDW calculations.

NUMERICAL EXAMPLES

Excitation to Magnetic Sublevels

The use of plasma polarization spectroscopy to diagnose plasma conditions has gained popularity in recent years [8–10]. Such diagnostics require a knowledge of collisional excitation cross sections among the magnetic sublevels of an ion. For example, consider the usual total angular momentum type of excitation transition ($J \rightarrow J'$) from the ground state of a He-like ion

$$e^- + (1s^2)_{J=0} \rightarrow e^{-'} + (1s\,2p_{1/2})_{J'=1}, \tag{5}$$

which can split into a number of transitions between specific magnetic sublevels ($M \rightarrow M'$)

$$e^- + (1s^2)_{J=0,M=0} \rightarrow e^{-'} + (1s\,2p_{1/2})_{J'=1,M'=0,\pm1}\,. \tag{6}$$

The polarization of light emitted from each of these excited states as they decay back down to the ground state has a different characterization, which can be used, for example, to obtain information about the nature of the electron energy distribution. Figure 1 provides a numerical example for this specific set of magnetic transitions in Fe^{24+} [11]. The total (i.e. $J \rightarrow J'$) collision strength, which can be obtained by summing the individual sublevel contributions in this case, is also provided as a reference to the next discussion concerning the resonance contribution to collisional excitation.

The Resonance Contribution to Collisional Excitation

In order to improve the accuracy of RDW calculations for less highly charged ions, it is necessary to include the effect of resonances, which can dominate the excitation cross section for small impact-electron energies. Once again considering excitation from the ground state of a He-like ion, it is possible to capture the incident electron to create an autoionizing level in the adjacent Li-like ion stage, which can then autoionize into an excited state of the He-like ion. Symbolically this resonance path can be written as

$$e^- + (1s^2)_{J=0} \rightarrow (1s\,3\ell\,3\ell')_{J''} \rightarrow e^{-'} + (1s\,2p_{1/2})_{J'=1}, \tag{7}$$

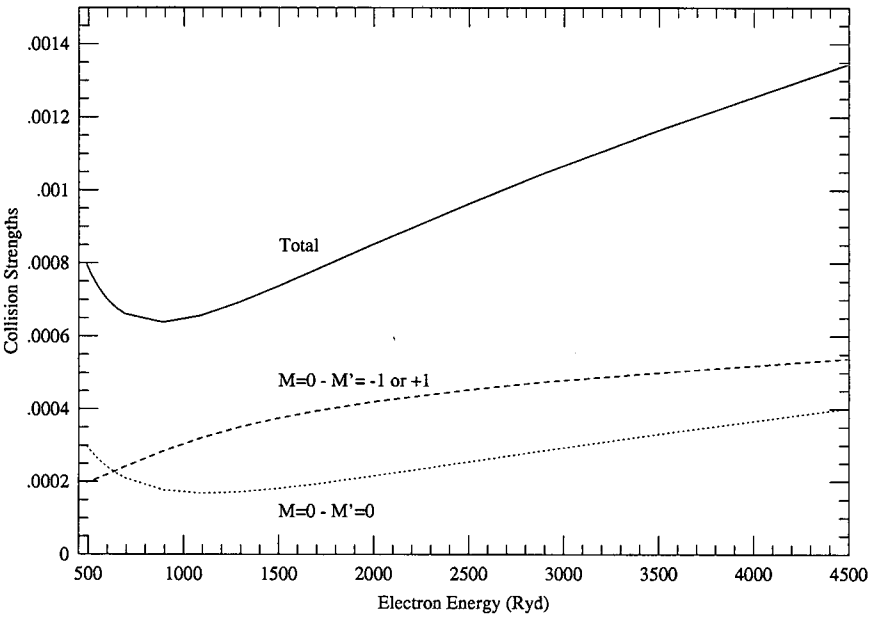

FIGURE 1: Magnetic sublevel and total collision strength for the $(1s^2)_0 \rightarrow (1s2p_{1/2})_1$ transition in He-like iron.

where only a small number of possible autoionizing levels (the so-called KMM resonances) have been listed explicitly. Figure 2 provides an example of the resonance contribution [11] for the same $(J \rightarrow J')$ transition displayed in Fig. 1. Note that the impact-electron energy range is only a small portion of that shown in Fig. 1. Figure 2 clearly shows the enhancement provided by resonance effects over the standard RDW calculation that is displayed by the smooth, "Total" curve in Fig. 1. Also provided in Fig. 2 is a more accurate R-Matrix calculation. The agreement between the RDW and R-Matrix results is considered to be quite good, giving some confidence that the RDW calculations can be improved using this two-step (or independent) process approach to the resonance contribution.

A Fully Relativistic Top-up Formulation for Collisional Excitation

When computing any type of DW cross section the partial-wave summation must be truncated at some orbital angular momentum value $\ell_{\max}$. There are a number of ways to estimate the remaining contribution from partial waves corresponding to $(\ell_{\max}+1)$ to ∞. This high-ℓ contribution is sometimes referred to as the "top-up". For relativistic calculations the top-up contribution is often obtained by hybridizing a nonrelativistic approach. Typically, the relativistic approach will

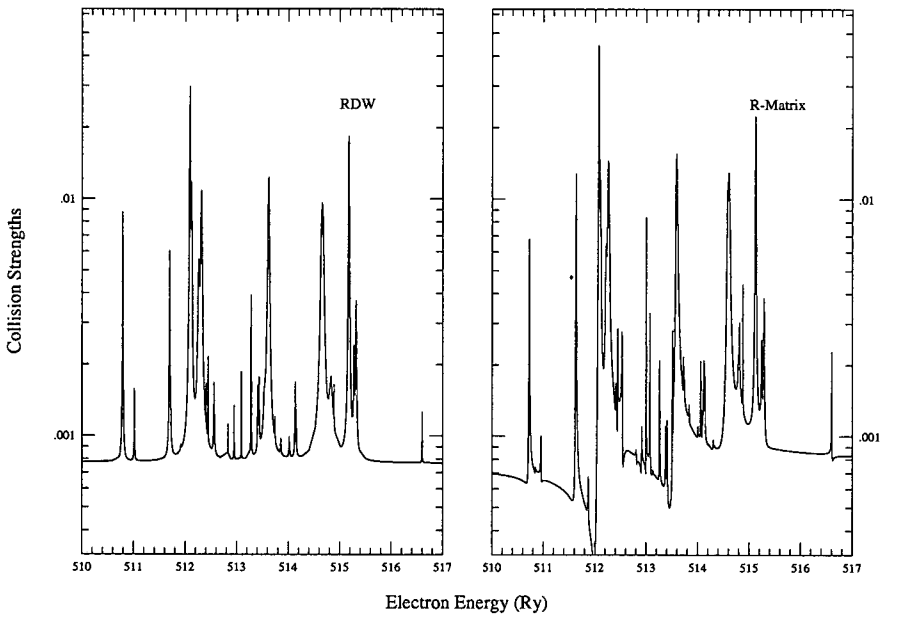

FIGURE 2: Total collision strength for the same transition described in Fig. 1, but with the resonance contribution included in the RDW calculation. An R-Matrix calculation is provided for comparisons.

have the same form as the nonrelativistic expression except that Dirac spinors, like those appearing in Eq. (1), are used to represent the bound electrons while the usual nonrelativistic wavefunctions are used for the continuum electrons. These so-called quasi-relativistic approaches have been employed, for example, when using the plane-wave-Born (PWB) approach to approximate the top-up for arbitrary transitions [12] and when using the Coulomb-Bethe approximation to estimate the top-up for dipole-allowed transitions [2].

In order to improve the top-up approximation in the LANL codes, a fully relativistic formulation has been developed [13] based on using relativistic PWB theory (RPWB) to estimate the high-ℓ contributions. As in the nonrelativistic case, an RDW cross section Q^{RDW} for a given transition may be written in the following general way

$$Q^{\mathrm{RDW}} = \sum_{\ell=0}^{\ell_{\max}} Q^{\mathrm{RDW}}(\ell) + Q^{\mathrm{TOP-UP}} \tag{8}$$

where $Q^{\mathrm{TOP-UP}}$ is to be approximated. Using RPWB theory it is possible to compute the total cross section $Q^{\mathrm{RPWB}}_{\mathrm{total}}$ (i.e. containing all partial-wave contributions, from ℓ=0 to ∞), in addition to the RPWB cross section $Q^{\mathrm{RPWB}}_{\ell_{\max}}$ that is computed by summing up partial-wave contributions from ℓ=0 to $\ell_{\max}$. Taking the difference

of these two RPWB cross sections provides an estimate of the top-up, which can be written as

$$Q^{\mathrm{TOP-UP}} \approx Q^{\mathrm{RPWB}}_{\mathrm{total}} - Q^{\mathrm{RPWB}}_{\ell_{\mathrm{max}}} = \sum_{\substack{\ell= \\ \ell_{\mathrm{max}}+1}}^{\infty} Q^{\mathrm{RPWB}}(\ell). \tag{9}$$

Approximating an infinite sum in this manner is sometimes referred to as the Kummer transformation, which appears as a label for the upper curve displayed in Fig. 3 to denote that the collision strength was obtained from this type of RPWB

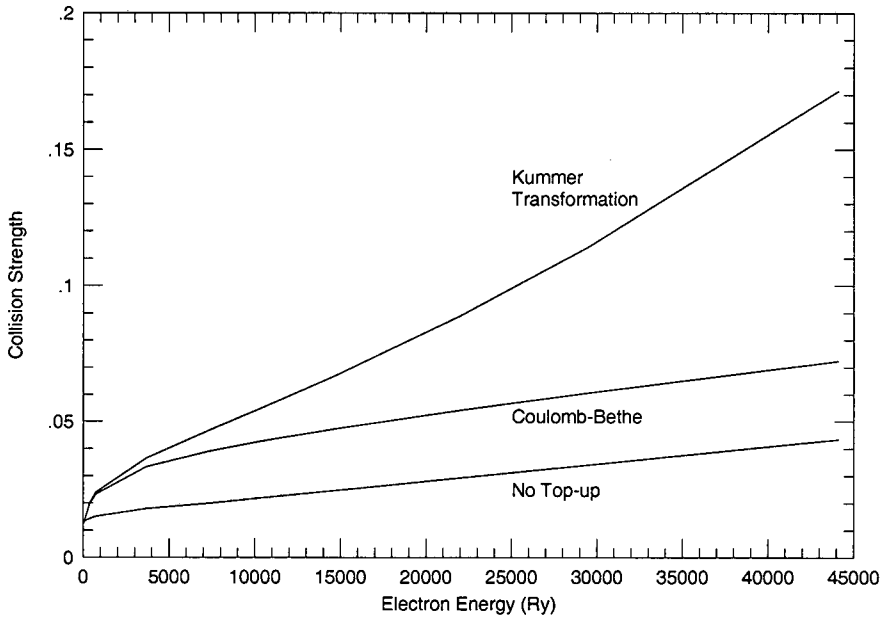

FIGURE 3: Collision strength for the $(1s\,2s)_1 \rightarrow (1s\,2p_{1/2})_1$ transition in He-like gold. The three curves represent the collision strength computed with the RPWB top-up, the Coulomb-Bethe approximation and no top-up.

top-up formulation. The figure also displays the collision strengths that result from either the quasi-relativistic, Coulomb-Bethe approximation mentioned above or no top-up treatment. For this example a Δn=0, dipole-allowed transition was chosen, which is the type of transition that typically has the largest top-up contribution. The He-like gold (Z=79) ion stage was chosen in order to accentuate relativistic effects. The large effects resulting from a fully relativistic top-up formulation are evident for this example.

The Generalized Breit Interaction

Another improvement to relativistic structure and scattering calculations involves the inclusion of the generalized Breit interaction (GBI) [14–17]. This interaction includes the lowest order QED effect represented by the exchange of a virtual photon and can be important when evaluating processes involving tightly bound electrons in high-Z elements. This two-electron interaction can be written in the form

$$\begin{aligned} g(1,2) &= \text{Coulomb interaction} + \text{generalized Breit interaction} \qquad (10) \\ &= \frac{1}{r_{12}} - (\boldsymbol{\alpha}_1 \cdot \boldsymbol{\alpha}_2)\frac{\exp(i\omega r_{12})}{r_{12}} + (\boldsymbol{\alpha}_1 \cdot \boldsymbol{\nabla}_1)(\boldsymbol{\alpha}_1 \cdot \boldsymbol{\nabla}_2)\frac{\exp(i\omega r_{12}) - 1}{\omega^2 r_{12}}, \end{aligned}$$

where ω is the frequency of the exchanged photon, the $\boldsymbol{\alpha}$ are the usual 4×4 Dirac matrices and $1/r_{12}$ is the usual Coulomb interaction which is added to the GBI to obtain the full two-electron interaction. The above formula results from choosing the Coulomb gauge. If the Feynman gauge is chosen, the Møller interaction [18] is obtained, which is also used to include the lowest order QED effect between two electrons in some computer codes.

A specific numerical example is presented in Fig. 4, where the cross section for collisional ionization of hydrogenic ions is displayed for three high-Z values (66, 79 and 92). The calculations were taken from [17] and the lone experimental point (for Z=92) was measured with the Lawrence Livermore EBIT apparatus, as discussed in [19]. Note the excellent agreement between experiment and theory at Z=92, underscoring the importance of the Breit interaction when calculating cross sections that involve tightly bound electrons in high-Z elements.

As expected, the behavior of the GBI is to increase the cross section over the entire range of impact energies, with the effect becoming more pronounced with increasing Z. The high-energy trends exhibited by these curves can be understood with some knowledge of the Bethe high-energy limit [20] that results from treating the continuum electrons as plane waves. The relativistic formula for the Bethe limit has the same form as the nonrelativistic formula, provided that one retains the impact electron velocity v instead of replacing it with the nonrelativistic (nr) expression for kinetic energy ($\varepsilon^{\rm nr} = mv^2/2$). For a transition of the form $J \rightarrow J'$ the relativistic, Bethe high-energy limit, ionization cross section has the form

$$Q^{\rm REL}_{J\rightarrow J'}(\varepsilon) \propto \frac{1}{mv^2}\ \log(C_{J\rightarrow J'}\, mv^2/\Delta E), \qquad (11)$$

where ΔE is the ionization energy and $C_{J\rightarrow J'}$ is a constant that can be determined from other fundamental atomic data that depend on the particular transition. Note that Eq. (11) includes ionization via the Coulomb interaction only. From this equation it is easy to understand why the curves computed with only the Coulomb interaction in Fig. 4 tend toward a constant value at high impact energies. As the

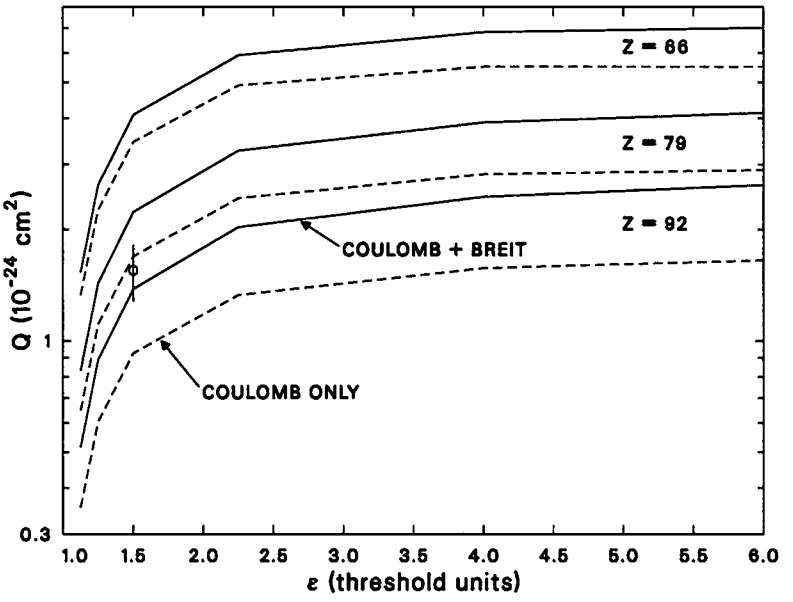

FIGURE 4: Ionization cross sections for the $1s$ electron in hydrogenic ions as a function of impact energy in threshold units. The dashed lines represent results calculated with only the Coulomb interaction while the solid lines represent the inclusion of both the Coulomb and Breit interactions. The circle with error bars represents the EBIT experimental value (for Z=92) listed in reference [19].

impact energy increases, the impact velocity v approaches the speed of light and so everything in Eq. (11) becomes constant.

Bethe went a step further [21] to include the effects of virtual photon exchange (i.e. the Breit interaction) in a perturbation expansion, retaining terms up to $O(v^2/c^2)$. The resulting ionization cross section

$$Q^{\mathrm{BREIT}}_{J\to J'}(\varepsilon) \propto \frac{1}{mv^2}\left[\log(C_{J\to J'}\, mv^2/\Delta E) - \log(1 - v^2/c^2) - v^2/c^2\right] \qquad (12)$$

contains two additional terms that do not appear in Eq. (11). These terms are sometimes referred to as the "relativistic rise", and it is straightforward to verify that they provide an increasingly positive contribution to the cross section with increasing impact energy, as displayed by the COULOMB+BREIT curves in Fig. 4.

Applications to Plasma Modeling

As stated at the beginning of this work, the ultimate goal of generating such large amounts of atomic data is to model non-LTE plasmas. For heavy elements

the size of relativistic atomic models (e.g. as measured by the number of configurations) can easily be more than an order of magnitude larger than the corresponding nonrelativistic models due to the jj-coupling that is required to describe relativistic subconfigurations. The computational requirements for such an effort strain existing resources and so the need to create fast, yet accurate, algorithms to carry out large-scale modeling calculations remains paramount.

Conferences, such as the recently held NLTE-3 Kinetics Workshop at NIST in Gaithersburg, MD [22], provide an opportunity to compare various approaches in solving a variety of test problems. Some of the test cases are experimentally motivated, while others are used strictly as benchmarks with which to compare theoretical calculations. The test case involving the heaviest element (gold) provides an excellent test bed for codes that can generate large amounts of relativistic data. For example, consider the emissivity plot displayed in Fig. 5 which represents a spectrum for a specific density/temperature point (N_e=10^{20} cm^{-3}, T_e=1.5 keV,

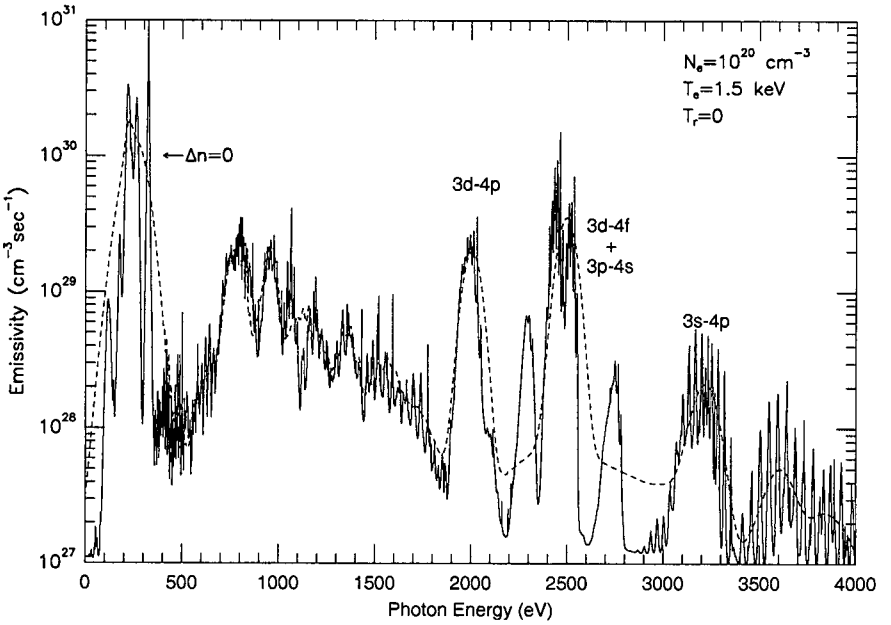

FIGURE 5: Emissivity for the NLTE-3 workshop, gold test case for the plasma conditions N_e=10^{20} cm^{-3}, T_e=1.5 keV, T_r=0.

T_r=0) prescribed by the gold test problem. The solid curve represents the emissivity computed from approximately 110,000 relativistic subconfigurations using the unresolved transition array (UTA) approach. The dashed curve represents the corresponding nonrelativistic curve computed from approximately 19,000 configurations. The relativistic model involved the calculation of millions of cross sections spanning eight ion stages (Ga-like through Sr-like) and required about

twenty hours of computational time (including the solution of the rate equations) on an SGI Origin 200 workstation. Even with this relatively large model the displayed spectrum is not fully converged. The exploration of still faster methods for generating atomic data and solving the rate equations remains a challenge for future research efforts.

This work was performed under the auspices of the US Department of Energy.

REFERENCES

1. D.H. Sampson, H.L. Zhang, A.K. Mohanty and R.E.H. Clark, *Phys. Rev. A* **40**, 604 (1989).
2. H.L. Zhang, D.H. Sampson and A.K. Mohanty, *Phys. Rev. A* **40**, 616 (1989).
3. H.L. Zhang, D.H. Sampson and R.E.H. Clark, *Phys. Rev. A* **41**, 198 (1990).
4. D.H. Sampson, H.L. Zhang and C.J. Fontes, "A Fully Relativistic Approach for Calculating Atomic Data for Highly Charged Ions", (in preparation for submission to Physics Reports).
5. J. Abdallah and R.E.H. Clark and J.M. Peek and C.J. Fontes, *J. Quant. Spect. Rad. Trans.* **51**, 1 (1994).
6. J. Abdallah, Jr., R.E.H. Clark, D.P. Kilcrease, G. Csanak and C.J. Fontes, *Atomic Processes in Plasmas*, Tenth Topical Conference, San Francisco, CA 1996, edited by A.L. Osterheld and W.H. Goldstein, AIP Conf. Proc. No. 381, (AIP, New York, 1996).
7. J. Abdallah Jr., H.L. Zhang, C.J. Fontes, D.P. Kilcrease and B.J. Archer, *J. Quant. Spect. Rad. Trans.* **71**, 107 (2001).
8. H.L. Zhang and D.H. Sampson, *Phys. Rev. A* **42**, 5378 (1990).
9. C.J. Fontes, H.L. Zhang and D.H. Sampson, *Phys. Rev. A* **59**, 295 (1999).
10. D.H. Sampson, H.L. Zhang, M.K. Inal and C.J. Fontes, in *Proceedings of the 3rd US-Japan Plasma Polarization Spectroscopy Workshop*, Livermore, CA June 18–21, 2001 (Edited by P. Beiersdorfer and T. Fujimoto), University of California Lawrence Livermore National Laboratory Report UCRL-ID-146907, p. 271.
11. H.L. Zhang and D.H. Sampson, *Phys. Rev. A* **66**, 042704 (2002).
12. Y.-K. Kim and P.S. Bagus, *Phys. Rev. A* **8**, 1739 (1973).
13. C.J. Fontes, LANL Research Note X-5:RN(U)-01-05 (LA-UR-01-2154), February 2001 (unpublished).
14. G. Breit, *Phys. Rev.* **39**, 616 (1932).
15. C.J. Fontes, D.H. Sampson and H.L. Zhang, *Phys. Rev. A* **47**, 1009 (1993).
16. C.J. Fontes, H.L. Zhang and D.H. Sampson, *Phys. Rev. A* **59**, 295 (1999).
17. C.J. Fontes, D.H. Sampson and H.L. Zhang, *Phys. Rev. A* **59**, 1329 (1999).
18. C. Møller, *Ann. Phys.* (Leipzig) **14**, 531 (1932).
19. C.J. Fontes, D.H. Sampson and H.L. Zhang, *Phys. Rev. A* **51**, R12 (1995).
20. M. Inokuti, *Reviews of Modern Physics* **43**, 297 (1971).
21. H. Bethe, *Z. Physik* **76**, 293 (1932).
22. Yu. Ralchenko et al., at this meeting (2004).